Sensors and Actuators B 254 (2018) 1242–1248

Contents lists available at ScienceDirect

Sensors and Actuators B: Chemical

journal homepage: www.elsevier.com/locate/snb

Doping effect on the sensing properties of ZnO nanoparticles for detection of 2-chloroethyl ethylsulfide as a mustard simulant

Ran Yoo, Dongmei Lee, Sungmee Cho, Wooyoung Lee*

Department of Materials Science and Engineering, Yonsei University, 262 Seongsanno, Seodaemun-gu, Seoul 129-749, Republic of Korea

ARTICLE INFO

Article history:
Received 7 November 2016
Received in revised form 4 June 2017
Accepted 12 July 2017
Available online 18 July 2017

Keywords:
Al-doped ZnO nanoparticles
2-Chloroethyl ethyl sulfide
Rapid response time
Gas sensor

ABSTRACT

In this work, we report the gas sensing properties of un-doped and M (M = Al, Co, Cu, Mn)-doped ZnO nanoparticles (NPs), synthesized by a hydrothermal method for the detection of 2-chloroethyl ethyl sulfide (2-CEES), as a mustard simulant. X-ray diffraction and X-ray photoelectron spectroscopy characterizations reveal that Al-doped ZnO NPs were successfully fabricated. The sensing response of 1 at% Al-doped ZnO NPs was found to be the maximum ($R = 954.2$) at 500 °C, owing to enhanced conductivity and concentration of the oxygen vacancies after Al doping. Al is a more effective dopant for ZnO NPs toward enhancing its sensing properties for the detection of 2-CEES than Cu, Co, or Mn. The Al-doped ZnO NPs are both sensitive and selective to 2-CEES. The sensing performance of these NPs for 2-CEES is approximately 15 times better than the ones reported previously for other types of NPs.

1. Introduction

Often used for military purposes to severely injure or incapacitate opposing forces, chemical warfare agents (CWAs) function by disrupting neurological regulation through acetylcholine esterase suppression. CWAs are classified as blister, nerve, choking, or behavioral altering agents and asphyxiants [1–3]. In particular, blister agents are dangerous in aerosol form and can contaminate a region for a long period, owing to their low volatility. An example of a blister agent is the mustard gas, which was commonly used in battlefields in the 20th century, including at Ypres, owing to simple and cost-effective production methods [1–3]. However, the unanticipated prolonged effect of CWAs on the civilians and environment led to the development of CWA detection using spectroscopic techniques such as nuclear magnetic resonance (NMR) [4], mass spectrometry [5,6], gas chromatography mass spectrometry (GC–MS) [7], and Raman spectroscopy [8,9]. However, these technologies are often complex and very expensive; thus, there is a need for a sensor that is more rapid and accurate compared to the analytical methods.

Metal oxide based sensors have been shown to possess the ability to detect very low concentrations of CWAs and simulants [10–12]. For instance, only few of the many metal oxide sensors, Pt-doped [13] and Ru-doped [14] $CdSnO_3$, have demonstrated the ability to detect 2-chloroethyl ethyl sulfide (2-CEES) gas as a simulant of mustard. $CdSnO_3$ thin films [14] used to detect 4 ppm of 2-CEES showed a sensing response of 12 at 350 °C, while Pt- and Ru-doped $CdSnO_3$ thin films exhibited enhanced sensing properties to 4 ppm of 2-CEES, with responses of 27 and 62 at 350 °C, respectively.

However, Pt- and Ru-doped $CdSnO_3$ films are known to be toxic and exhibit a slow response time to 2-CEES [2,3]. ZnO is an alternative promising material for gas sensors, owing to its high thermal and chemical stabilities, abundance, and better sensing properties [15,16]. By controlling the structure and morphologies of nanoparticles [17], nanowires [18], nanorods [19], and nanosheets [20], the performance of gas sensors has been greatly accelerated. Additional approaches have been used to produce three-dimensional (3D) structures, to further enhance their sensing properties [21], as they provide a large surface area to volume ratio that enables greater gas diffusion and mass transport in the sensors. Furthermore, sensing properties can be improved by introducing dopants into the metal oxide sensing materials, thereby enhancing their electrical conductivities. Various dopants (*e.g.*, Al, In, Pt, Pd, and Co) can alter the sensing properties by altering the morphology and energy band structures, and generating more sites for gas interaction on the surface [22]. Sensors based on Al-doped ZnO NPs [15] have been reported to exhibit excellent sensing response, owing to the Al doping effect, to dimethyl methylphosphonate as a simulant of Sarin. Doping Al into the ZnO crystal structure can alter its band structure due to the substitution of Al^{3+} ions (0.53 Å) at the Zn^{2+} ion (0.74 Å) sites [23], leading to enhanced conductivity of the

* Corresponding author.
E-mail address: wooyoung@yonsei.ac.kr (W. Lee).

http://dx.doi.org/10.1016/j.snb.2017.07.084
0925-4005/

host material [22]. Furthermore, the Al dopant promotes abundant oxygen vacancies in the ZnO.

In this work, we investigated the gas sensing properties of un-doped and M (M = Al, Cu, Co, Mn)-doped ZnO nanoparticles (NPs) synthesized by a hydrothermal method for the detection of 2-CEES. We found that the incorporation of Al into the ZnO crystal structure results in enhanced conductivity and concentration of oxygen vacancies, improving the sensing response of the ZnO NPs. The related mechanism is also addressed in detail.

2. Material and methods

2.1. Un-doped and M (M = Al, Cu, Co, Mn)-doped ZnO NPs synthesis and device fabrication

Un-doped and M (M = Al, Cu, Co, Mn)-doped ZnO NPs were synthesized by a hydrothermal method. In general, hydrothermal synthesis is well known to crystallize substances from high-temperature aqueous solutions at high vapor pressures. However, we hydrothermally synthesized the ZnO NPs at a relatively low temperature (60 °C) under air pressure, as reported in a previous work [24,25]. Zinc acetate dihydrate ($Zn(CH_3COO)_2{\cdot}2H_2O$, Sigma-Aldrich) was first dissolved in methanol to form a 0.205 M solution, and potassium hydroxide (KOH, Sigma-Aldrich) was dissolved in methanol to form a 0.06 M solution [15]. For the synthesis of Al-doped ZnO NPs, aluminum acetate ($Al(C_2H_3O_2)_3$, Sigma-Aldrich) was added to the zinc acetate solution, at various atomic ratios of the dopant to Zn, 0.5, 1.0, 1.5, and 2.0 at%. The KOH solution was mixed with the zinc precursor solution by stirring at 60 °C for 24 h. The suspension of the particles was centrifuged and washed thrice with methanol and dried at 90 °C for 60 min. The dried samples were finally annealed at 350 °C for 30 min in a H_2/N_2 atmosphere. According to a previous report [26], the annealing process changes the carrier concentration and mobility of a ZnO film annealed in hydrogen atmosphere. This is because of the evolution of charge carriers and the enhancement of charge transport by the generation of defect states such as oxygen vacancies [27].

For the fabrication of sensors, both Cr (20 nm) and Pt (100 nm) layers were deposited on the patterned SiO_2 substrate, *via* a DC sputtering system [15]. The Cr layer was used as an interlayer to provide a good contact between the Pt thin film and the SiO_2 substrate. The un-doped and Al-doped ZnO NPs were mixed with α-terpineol binder and spread on the interdigitated Pt electrode. The samples were dried at 300 °C for 1 h, and annealed subsequently at 600 °C for 1 h for the removal of the binding agent.

2.2. Structural characterization

The synthesized nanoparticles were structurally characterized by X-ray diffraction (XRD, Ultima IV/ME 200DX, Rigaku). The size and crystalline structure were investigated by field-emission scanning electron microscopy (FE-SEM, JEOL 7001F), transmission electron microscopy (TEM, JEOL JEM ARM 200F) with energy dispersive X-ray spectroscopy (EDX, X Max Oxford), and X-ray photoelectron spectroscopy (XPS, K-alpha Thermo VG). XPS was carried out using Al Kα radiation (1486.6 eV) from an X-ray source operated at 12 kV with a current of 3 mA.

2.3. Gas sensing measurements

A device was mounted in a chamber and placed in a flow system equipped with gas cylinders and mass flow controllers (MFCs) to perform the gas sensing test. The mixture of 2-CEES gas and air was controlled by varying the gas flow rates produced by MFCs. The

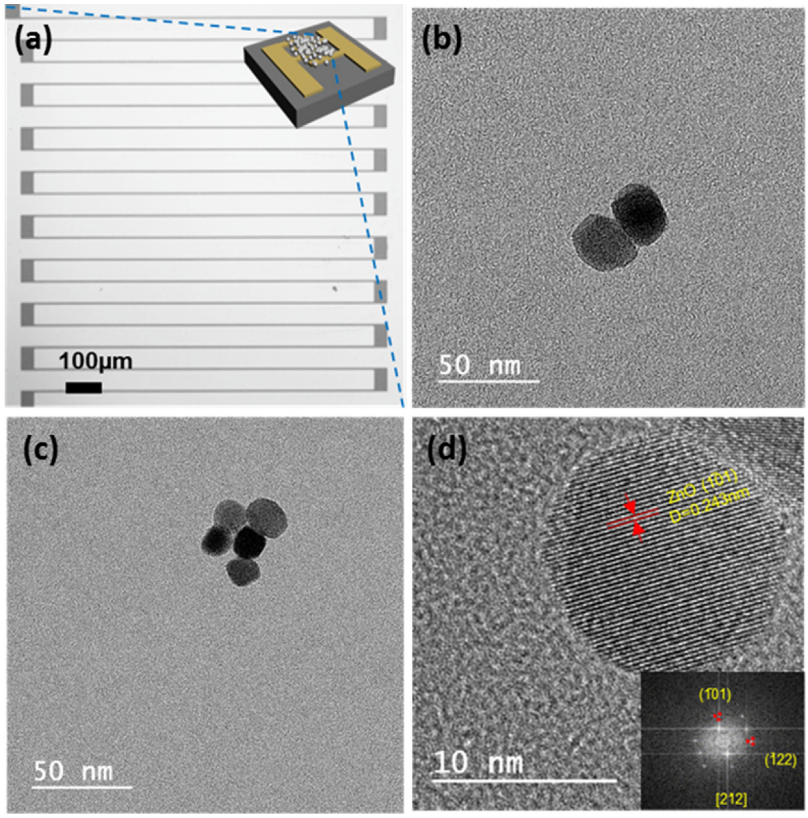

Fig. 1. (a) A schematic of the sensor device, and SEM image of an actual Pt electrode; TEM images of (b) un-doped and (c) 1 at% Al-doped ZnO NPs and (d) an Al doped ZnO grain showing the lattice structure and the corresponding electron diffraction pattern.

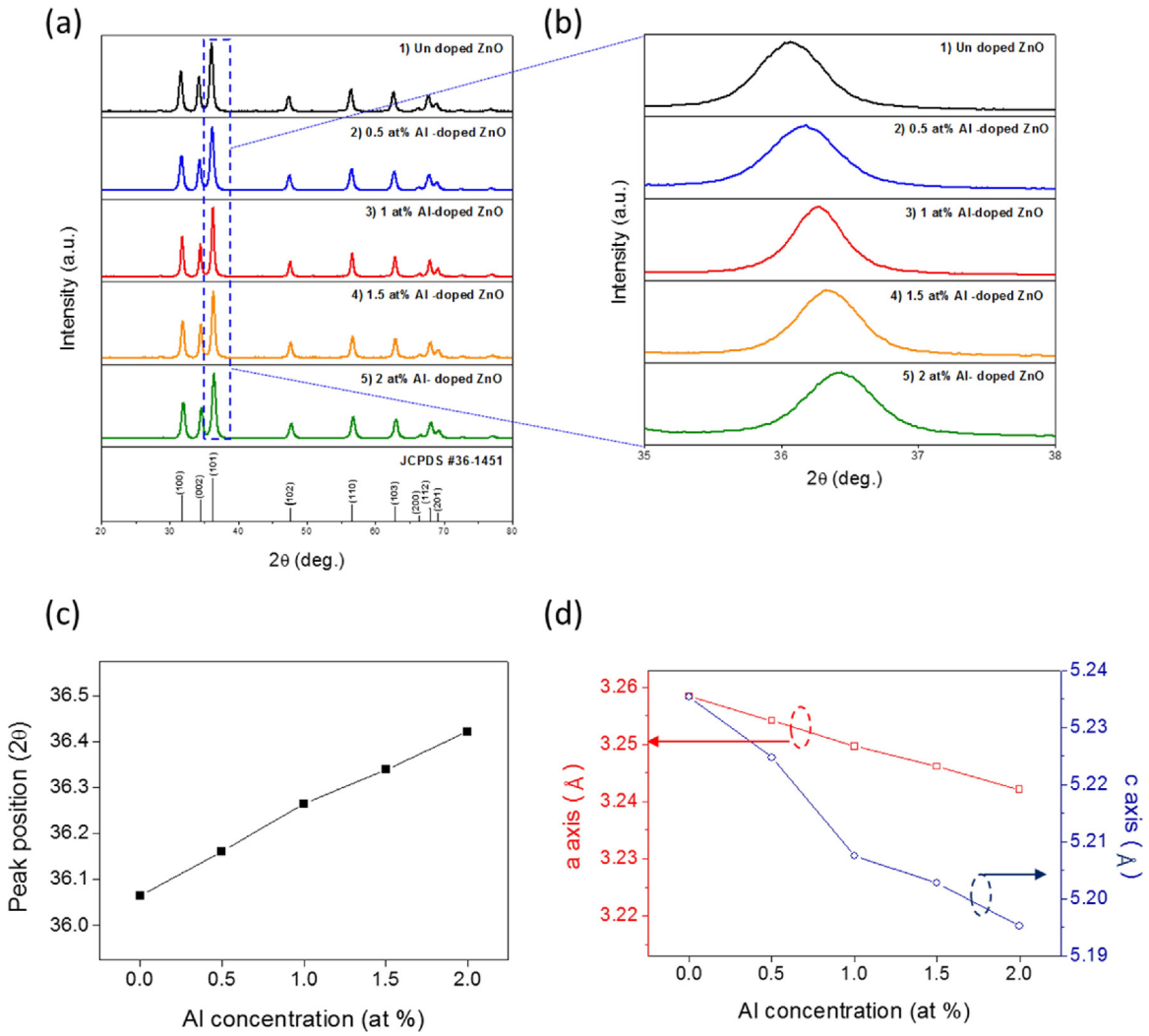

Fig. 2. (a) X-ray diffraction (XRD) patterns, (b) magnified (101) peaks, (c) (101) peak position, and (d) lattice parameters *a* and *c* as a function of the Al content for un-doped and doped ZnO NPs.

sensing properties were measured using a combination of a current source (Keithley 6220) and a nanovoltmeter (Keithley 2182) with a constant current supply of 10 nA for a time interval of 1 s. All the gas sensing measurements were conducted at operating temperatures of 300–525 °C. The sensing response for the 2-CEES gas is defined as $(R_{air} - R_{gas})/R_{gas}$, where R_{gas} and R_{air} are the resistances of the sensor in an environment containing 2-CEES and plain air, respectively. The response time is defined as the time required to reach 90% of the total resistance change, upon exposure to the test gas. The recovery time is defined as the time required to revert to 10% of the original resistance in standard air condition, upon release of the test gas.

3. Results and discussion

The sensor device (8.5 mm × 8.5 mm) was fabricated by depositing interdigitated Pt electrodes on a Si/SiO_2 substrate, as shown in Fig. 1(a). The magnified Pt electrodes on the right show a highly interdigitated array with a periodic spacing of 5 μm between the Pt layers, as shown in the inset of Fig. 1. Fig. 1(b) shows that the un-doped ZnO NPs are spherical with a diameter of ~30 nm. However, the Al-doped ZnO (<25 nm) NPs display slightly smaller grains compared to the un-doped ZnO NPs (~30 nm). Owing to the smaller grain size, the Al-doped ZnO NP has a larger surface area than the un-doped ZnO NP, indicating that the enhanced sensing response of the Al-doped ZnO NPs can be related to the grain size effect [28,29]. An Al-doped ZnO grain shown in Fig. 1(d) presents a lattice parameter of 0.243 nm, corresponding to the (101) planes of wurtzite ZnO. The indexed FFT (fast Fourier transformation) pattern along the [21 $\bar{2}$] zone axis in the inset of Fig. 1(d) indicates that the Al-doped ZnO grain has a hexagonal wurtzite structure.

Fig. 2 shows (a) X-ray diffraction (XRD) patterns, (b) magnified (101) peaks, (c) the (101) peak position, and (d) lattice parameters *a* and *c* of the ZnO NPs as a function of Al content. All the peaks in the XRD patterns of un-doped and doped ZnO NPs indicate that ZnO (JCPDS: # 36-1451) formed a hexagonal wurtzite phase without any secondary phase. As the Al content increased, the main (101) peak position in all the doped samples was observed to shift to slightly larger angles compared to that of the un-doped ZnO NPs (see in Fig. 2(b)). The (101) peak position is plotted in Fig. 2(c). The peak position shifted linearly to a larger angle with increasing Al content, indicating that the doping of Al into the ZnO NP reduces the *d*-spacing along the [101] direction. This is due to Al^{3+} (ionic radius 0.53 Å) effectively substituting Zn^{2+} (ionic radius 0.74 Å) in the wurtzite structure [23]. The lattice parameters of the *a*-axis and *c*-axis decrease with increasing Al content up to 2 at% (Fig. 2(d)). The lattice parameter of the *c*-axis decreases more than that of the *a*-axis, owing to the hexagonal crystal system.

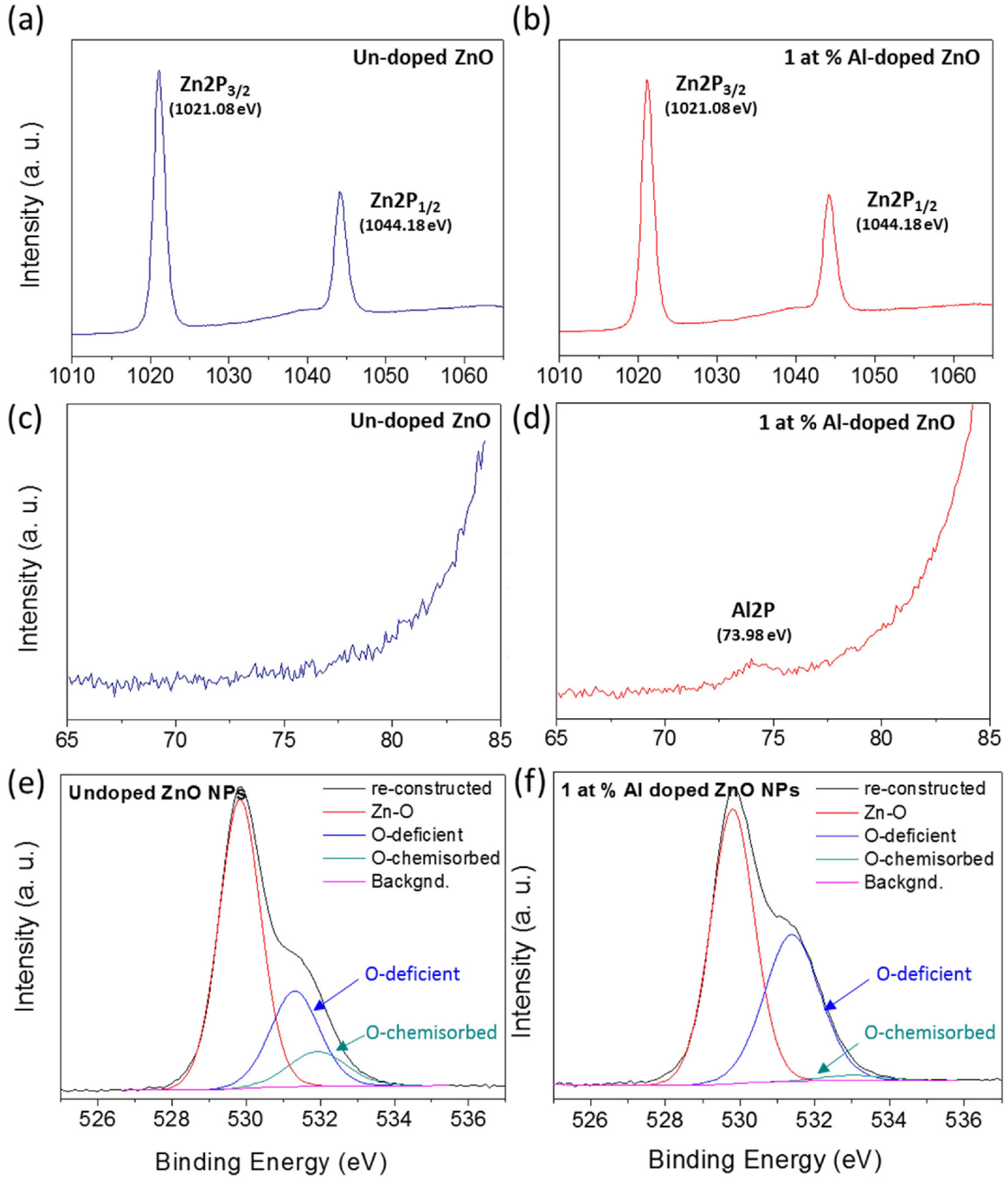

Fig. 3. XPS spectra of un-doped and 1 at% Al-doped ZnO NPs: (a, b) Zn 2p spectra (c, d) Al 2p spectra and (e, f) convoluted O 1s spectra.

Fig. 3 exhibits XPS spectra of un-doped ZnO NPs: (a) Zn 2p spectra (c) Al 2p spectra and (e) convoluted O 1s spectra, and XPS spectra of 1 at% Al doped ZnO NPs: (b) Zn 2p spectra (d) Al 2p spectra and (f) convoluted O1s spectra. Fig. 3(a) and 3(b) show two Zn 2p peaks at 1021.08 and 1044.08 eV, corresponding to the binding energies of Zn $2p_{3/2}$ and Zn $2p_{1/2}$ in the un-doped and Al-doped ZnO NPs, respectively [30]. However, Fig. 3(c) does not show Al 2p peak for the un-doped ZnO NPs while Fig. 3(d) shows an Al 2p peak at 73.98 eV for the Al-doped ZnO NPs. The Al 2p peak at 73.98 eV corresponds to the Al–O bond formed in the crystal structure of ZnO [31] which is not related to the metallic Al (~72 eV) or a secondary phase such as Al_2O_3 (above 75 eV), implying that Al exists only in the oxidized state. Also, according to the XPS analysis, when 1 at% of Al is introduced to the Zn solution, the actual doping concentration in the particles is 0.23 at%. The real doping concentration increases up to 0.6 at% upon increasing the Al content up to 2.0 at% in the Zn solution (not shown). In the literature, an experimental solubility limit has been estimated under 0.3 at% of Al using X-ray diffraction refinements or NMR analysis [32,33]. In general, the product formed in a chemical reaction does not follow the stoichiometric equation. Therefore, during the synthesis process, Al not doped into ZnO is removed by a cleaning process. This can be verified by confirming the absence of secondary phase peaks and metallic ion peaks of Al in XRD and XPS.

Fig. 3(e) and (f) display reconstructed and deconvoluted O 1s XPS peak for un-doped and Al-doped ZnO NPs, respectively. The

red, blue, and green lines are deconvoluted from reconstructed O 1s peak to investigate the change in the oxygen vacancy in ZnO after Al doping. The peak close to 530 eV (red-line) is attributed to the O 1s level in the ZnO wurtzite structure surrounded by Zn (or substituted Al) atoms with their nearest-neighbor O^{2-} ions. The peak is close to 531.4 eV, (blue-line) implying that the oxygen ions are in the oxygen deficient regions (oxygen vacancy), referred as O-deficient. Further, a peak with a binding energy of 532 eV (green-line) indicates the presence of oxygen ions on the surface of the ZnO, belonging to certain oxygen containing species such as adsorbed O_2, H_2O, CO_2, referred as O-chemisorbed [34,35]. We found that the concentration of the oxygen vacancy increases to maintain the electrical neutrality after the doping of Al into the ZnO matrix.

Fig. 4 shows (a) the sensing response of the Al-doped ZnO NPs as a function of the Al content (0, 0.5, 1.0, 1.5, and 2.0 at%) to 20 ppm of 2-CEES at 500 °C, (b) change in the sensing response of the un-doped and the Al-doped ZnO NPs in the range of 300–525 °C to 20 ppm of 2-CEES, and (c) the sensing response for 1 at% Al, Cu, Co, and Mn-doped ZnO NPs at 500 °C. The representative sensing response behaviors of the Al-doped ZnO NPs as a function of the Al content (0, 0.5, 1.0, 1.5, and 2.0 at%) are presented in Fig. 4(a), showing that the responses from un-doped and doped ZnO NPs increase rapidly upon exposure to 2-CEES. The inset of Fig. 4(a) exhibits the sensing response as a function of the Al content (0, 0.5, 1.0, 1.5, and 2.0 at%). The response of Al-doped ZnO NPs was observed to increase up to 1 at% and then decrease for 1.5 at% Al content. The highest sensing response of 954.2 was observed for 20 ppm of 2-CEES at 500 °C with 1 at% Al-doped ZnO NPs. The sensing performance of the Al-doped ZnO NPs for 2-CEES is approximately 15 times higher than those of $CdSnO_2$ [14], Ru-doped $CdSnO_2$ [13], and Pt-doped $CdSnO_2$ [14].

In the absence of the target gas (*e.g.*, in air), the oxygen molecules can adsorb on the surface of the nanoparticles and receive electrons from the conduction band to generate chemisorbed oxygen species such as O^{2-} and O^- at higher temperatures, which results in an increase in the resistance of the ZnO NPs, as the thickness of the depletion layer increases. Conversely, in the presence of 2-CEES, the exchange of charge between 2-CEES and the oxygen species (O^{2-}) absorbed on the ZnO surface leads to a variation in the charge depletion layer, *i.e.*, an increase in the surface barrier height in the conduction band. Therefore, the thickness of the depletion layer and the resistance of the ZnO NPs are decreased [13,14].

We found that the electrical resistance in air for the Al doped ZnO NPs decreases with doping concentration up to 1 at% Al and then increases. The decrease in the electrical resistance is attributed to the additional electrons owing to the formation of a donor level by the Al dopant [36,37]. Thus, more oxygen ions can adsorb on the surface of the Al doped ZnO NPs due to increased electrons. Therefore, greater quantity of 2-CEES molecules chemically react with the oxygen ions on the surface of the Al doped ZnO NPs, leading to enhanced sensing response in 1 at% Al doped ZnO NPs. However, the sensing response decreases at dopant concentrations higher than 1 at% owing to increased electron scattering in the ZnO crystal, because of disorder produced in the lattice of the ZnO crystal [38]. The highest response obtained from 1 at% Al-doped ZnO NPs also can be explained by the presence of more oxygen vacancies owing to Al doping. These act as adsorption sites for 2-CEES on the surface of the ZnO NPs, as shown in Fig. 3(e) and (f).

The sensing response of the Al-doped ZnO NPs significantly increases with increasing operating temperature up to 500 °C, and then decreases at 525 °C, as shown in Fig. 4(b). The inset of Fig. 4(b) shows a decrease in the electrical resistance of the 1 at% Al doped ZnO NPs with increasing temperature in the range of 300–525 °C, which is attributed to the intrinsic properties of semiconducting metal oxides with increasing temperature. The decreased response at 525 °C can be due to the competing desorption of the chemisorbed oxygen on the surface of the ZnO NP [39,40].

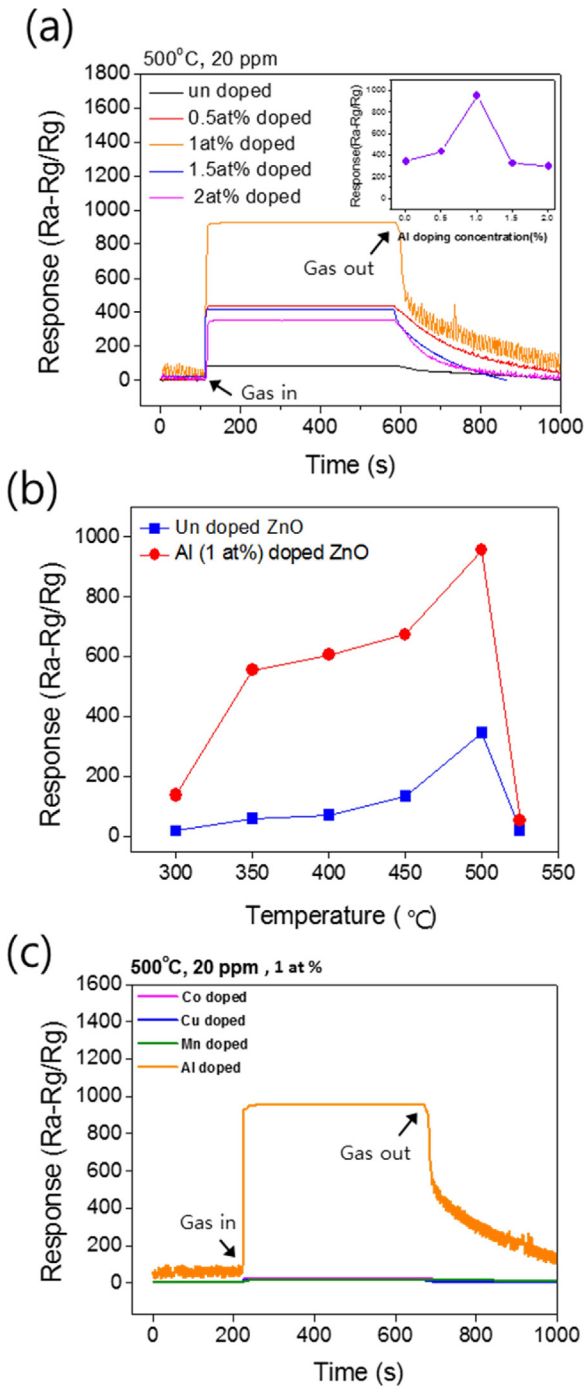

Fig. 4. (a) Sensing response of the Al-doped ZnO NPs as a function of the Al content (0, 0.5, 1.0, 1.5, and 2.0 at%) to 20 ppm of 2-CEES at 500 °C, (b) variation in the sensing responses of the un-doped and the Al-doped ZnO NPs in the range 300–525 °C, for 20 ppm of 2-CEES, and (c) sensing responses of 1 at% Al, Cu, Co, and Mn-doped ZnO NPs at 500 °C.

Fig. 4(c) presents the sensing response of ZnO NPs with 1 at% Al, Cu, Co, and Mn at 500 °C to 20 ppm of 2-CEES. The sensing response of Al-doped ZnO NPs is much higher than those of the ZnO NPs doped with other elements (Cu, Co, and Mn) owing to the difference in the valence electrons between Al and the other elements. In other words, Zn has two valence electrons and all the other elements have two valence electrons, except for Al, which has three valence electrons. After the substitution of Zn^{2+} by Al^{3+}, the additional electron

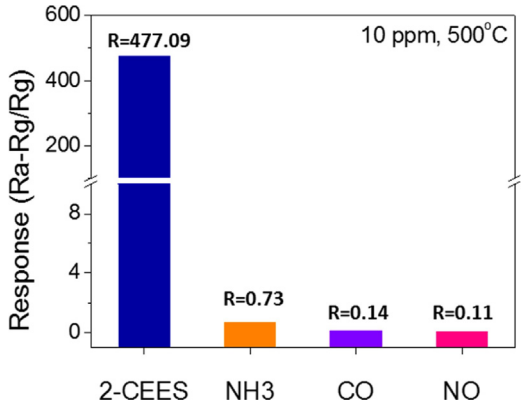

Fig. 5. The sensing responses of 1 at% Al-doped ZnO NPs to 10 ppm of 2-CEES and other gases (NH_3, CO, and NO) at 500 °C.

is bound loosely owing to the weak electrostatic attraction force around the Al. Therefore, the donor level forms below the conduction band of ZnO owing to the additional electrons playing the role of conduction electrons. Therefore, Al is an effective dopant for ZnO NPs with high sensing ability for 2-CEES.

Fig. 5 exhibits the sensing response for 1 at% Al-doped ZnO NPs to 10 ppm of 2-CEES and other gases (NH_3, CO, and NO) at 500 °C. The Al-doped ZnO NPs show much higher response to 2-CEES than NH_3, CO, and NO, indicating that the Al-doped ZnO NPs are very selective for 2-CEES compared to NH_3, CO, and NO. This is due to the larger dipole moment in the molecular structure of 2-CEES (2.25 D) than NH_3 (1.47 D), CO (0.122 D), and NO (0.16 D) [41].

4. Conclusions

We investigated the effect of doping on the sensing properties of ZnO NPs synthesized using a hydrothermal method for the detection of 2-CEES. We found from XRD and XPS results that Al-doped ZnO NPs were successfully fabricated. The 1 at% Al-doped ZnO NPs showed the maximum sensitivity (R = 954.2) at 500 °C due to enhanced conductivity and concentration of oxygen vacancies after Al doping. The enhanced conductivity is due to additional electrons in the system, owing to the formation of a donor level by Al doping, and the increase in the oxygen vacancy to maintain the electrical neutrality in ZnO after Al doping. The doping of Al into ZnO NPs is the most effective in enhancing its sensing properties for the detection of 2-CEES compared to other dopants such as Cu, Co, and Mn, owing to the differences in the valance electrons. The Al-doped ZnO NPs show much higher response to 2-CEES than NH_3, CO, and NO, owing to the larger dipole moment in the molecular structure of 2-CEES than in NH_3, CO, or NO. Our results demonstrate that the Al-doped ZnO NPs are both sensitive and selective to 2-CEES.

Funding

This work was supported by the Agency for Defense Development (ADD) of the Republic of Korea and Priority Research Centers Program (2009-0093823) through the National Research Foundation of Korea (NRF) and Korea Ministry of Environment as “Convergence Technology Program (2015001650001)”.

References

[1] K. Ganesan, S.K. Raza, R. Vijayaraghavan, J. Pharm. Bioallied Sci. 2 (2010) 166–178.
[2] S. Chauhan, R. D'Cruzf, S. Faruqi, K.K. Singh, S. Varma, M. Singh, V. Karthik, Environ. Toxicol. Pharmacol. 26 (2008) 113–122.
[3] K. Kim, O.G. Tsay, D.A. Atwood, D.G. Churchill, Chem. Rev. 111 (2011) 5345–5403.
[4] W.T. Beaudry, G.W. Wagner, J.R. Ward, J. Mol. Catal. 73 (1992) 77–90.
[5] C. Hsu, C.S. Dulcey, J.S. Horwitz, M.C. Lin, J. Mol. Catal. 60 (1990) 389–398.
[6] J.H. Werner, T.A. Cool, Chem. Phys. Lett. 275 (1997) 278–282.
[7] R.S. Pilling, G. Bernhardt, C.S. Kim, J. Duncan, C.B. Crothers, D. Kleinschmidt, D.J. Frankel, R.J. Lad, B.G. Frederick, Sens. Actuators B: Chem. 96 (2003) 200–214.
[8] N. Taranenko, J. Pierre, D. Stokes, T. Vo-Dinh, J. Raman Spectrosc. 27 (1996) 379–384.
[9] D.E. Tevault, R.E. Pellenbarg, Sci. Total Environ. 73 (1988) 65–69.
[10] G. Sberveglieri, C. Baratto, E. Comini, G. Faglia, M. Ferroni, M. Pardo, A. Ponzoni, A. Vomiero, Thin Solid Films 517 (2009) 6156–6160.
[11] S.C. Lee, H.Y. Choi, S.J. Lee, W.S. Lee, J.S. Huh, D.D. Lee, J.C. Kim, Sens. Actuators B: Chem. 137 (2009) 239–245.
[12] S.C. Lee, H.Y. Choi, W.S. Lee, S.J. Lee, D. Ragupathy, D.D. Lee, J.C. Kim, Sens. Lett. 9 (2011) 101–105.
[13] L.A. Patil, V.V. Deo, M.D. Shinde, A.R. Bari, M.P. Kaushik, Sens. Actuators B: Chem. 160 (2011) 234–243.
[14] L.A. Patil, V.V. Deo, M.D. Shinde, A.R. Bari, D.M. Patil, M.P. Kaushik, Sens. Actuators B: Chem. 191 (2014) 130–136.
[15] R. Yoo, J. Kim, M.-J. Song, W. Lee, J.S. Noh, Sens. Actuators B: Chem. 209 (2015) 444–448.
[16] M. Yin, S. Liu, Mater. Chem. Phys. 149 (2015) 344–349.
[17] P. Rai, Y.T. Yu, Sens. Actuators B: Chem. 173 (2012) 58–65.
[18] C.L. Hsu, K.C. Chen, T.Y. Tsai, T.J. Hsueh, Sens. Actuators B: Chem. 182 (2013) 190–196.
[19] T.R. Rashid, D.T. Phan, G.S. Chung, Sens. Actuators B: Chem. 185 (2013) 777–784.
[20] S.-L. Zhang, J.-O. Lim, J.-S. Huh, J.-S. Noh, W. Lee, Curr. Appl. Phys. 13 (2013) S156–S161.
[21] M.R. Alenezi, S.J. Henley, N.G. Emerson, S. Ravi, P. Silva, Nanoscale 6 (2014) 235–247.
[22] N.L. Hadipour, A.A. Peyghan, H. Soleymanabadi, J. Phys. Chem. 119 (2015) 6398–6404.
[23] P.P. Sahay, R.K. Nath, Sens. Actuators B: Chem. 134 (2008) 654–659.
[24] W. Guo, T. Liu, R. Sun, Y. Chen, W. Zeng, Z. Wang, Sens. Actuators B: Chem. 178 (2013) 53–62.
[25] X. Chen, X. Jing, J. Wang, J. Liu, D. Song, Superlattices Microstruct. 63 (2013) 204–214.
[26] H.-W. Park, K.-B. Chung, J.-S. Park, Curr. Appl. Phys. 12 (2012) S164.
[27] J. Kim, M.-C. Kim, J. Yu, K. Park, Curr. Appl. Phys. 10 (2010) S495.
[28] C. Xu, J. Tamaki, N. Miura, N. Yamazoe, Sens. Actuators B: Chem. 3 (2) (1991) 147–155.
[29] Y.-F. Sun, S.-B. Liu, F.-L. Meng, J.-Y. Liu, Z. Jin, L.-T. Kong, J.-H. Liu, Sensors 12 (2012) 2610–2631.
[30] J. Wang, Yang Li, Y. Kong, J. Zhou, J. Wu, X. Wu, W. Qin, Z. Jiao, L. Jiang, RSC Adv. 5 (2015) 81024–81029.
[31] J.T. Chen, J. Wang, R.F. Zhuo, D. Yan, J.J. Feng, F. Zhangand, P.X. Yan, Appl. Surf. Sci. 255 (2009) 3959–3964.
[32] D. Nie, T. Xue, Y. Zhang, X. Li, Sci. China Ser. B: Chem. 51 (9) (2008) 823–828.
[33] H. Serier, M. Gaudon, M. Míeníetrier, Solid State Sci. 11 (7) (2009) 1192–1197.
[34] S. Yun, S. Lim, et al., J. Solid State Chem. 184 (2011) 273–279.
[35] S. Bai, T. Guo, Y. Zhao, R. Luo, D. Li, A. Chen, C.C. Liu, J. Mater. Chem. A 1 (2013) 11335–11342.
[36] P. Banerjee, W.-J. Lee, K.-R. Bae, S.B. Lee, G.W. Rubloff, J. Appl. Phys. 108 (2010) 043504.
[37] A. Nakrela, N. Benramdane, A. Bouzidi, Z. Kebbab, M. Medles, C. Mathjeu, Results Phys. 6 (2016) 133–138.
[38] W.G. Chen, T.Y. Gao, H.L. Gan, L.N. Xu, L.F. Jin, Mater. Technol.: Adv. Perform. Mater. 30 (6) (2015) 356–361.
[39] L.-J. Bie, X.-N. Yan, J. Yin, Y.-Q. Duan, Z.-H. Yuan, Sens. Actuators B: Chem 126 (2007) 604–608.
[40] L.-J. Bie, Z.-N. Yan, J. Yin, Y.-Q. Duan, Z.-H. Yuan, Sens. Actuators B: Chem. 126 (2007) 604–608.
[41] G.J. Francis, D.B. Milligan, M.J. McEwan, Anal. Chem. 81 (21) (2009) 8892–8899.

Biographies

Ran Yoo earned her Master's Degree in 2013. She is currently studying on the nerve agent gas sensor using carbon nanotubes or metal oxide toward her ME in Nerve Agent Gas sensor at Yonsei University.

Sungmee Cho earned his Ph.D. degree in Electrical Engineering in 2011 from Texas A&M University. She was postdoc researcher at Materials Science & Engineering at Northwestern University in 2011–2012. She has been with Doosan Corporation as a researcher in 2003–2004 and Korea Institute Science Engineering (KIST) as are searcher in 2002–2003 and 2004–2005. Now she is a research professor in Materials Science and Engineering at Yonsei University. Her current research interests include Mg2Si-based thermoelectric (TE) energy conversion, TE module joint, thin film hydrogen storage, hydrogen gas sensor, solid oxide fuel cell (SOFC), and Li ion battery.

Wooyoung Lee is a Professor of Department of Materials Science and Engineering at Yonsei University in Korea. He received a BS degree in metallurgical engineering from the Yonsei University in 1986, a MS degree in metallurgical engineering from the Yonsei University in 1988. He received a Ph.D. degree in Physics from University of Cambridge, England in 2000. He is also the Chairman in University Industrial Technology Force (UNITEF), and a Member of the National Council on Science and Technology. In recent years, his research interests have centered on thermoelectric devices, spintronics and hydrogen sensors based on nanowires. He has received a number of awards in nano device-related research areas, including a Service Merit Medal (2008) due to contribution on the development of intellectual properties. He has authored and co-authored over 150 publications, and has edited a few of special books on nano-structured materials and device.